Heliyon 9 (2023) e21894

Contents lists available at ScienceDirect

Heliyon

journal homepage: www.cell.com/heliyon

Multifunctional effect of flavonoids from *Millettia brandisiana* against Alzheimer's disease pathogenesis

Puguh Novi Arsito [a,b], Pornthip Waiwut [c], Chavi Yenjai [d], Supakorn Arthan [e], Orawan Monthakantirat [a], Natsajee Nualkaew [a], Pitchayakarn Takomthong [a], Chantana Boonyarat [a,f,*]

[a] *Faculty of Pharmaceutical Sciences, Khon Kaen University, Khon Kaen, 40002, Thailand*
[b] *School of Pharmacy, Faculty of Medicine and Health Sciences, Universitas Muhammadiyah Yogyakarta, Yogyakarta, 55183, Indonesia*
[c] *Faculty of Pharmaceutical Sciences, Ubon Ratchathani University, Ubon Ratchathani, 34190, Thailand*
[d] *Natural Products Research Unit, Department of Chemistry and Center of Excellence for Innovation in Chemistry, Faculty of Science, Khon Kaen University, Khon Kaen, 40002, Thailand*
[e] *Program of Chemistry, Faculty of Science and Technology, Sakon Nakhon Rajabhat University, Mueang District, Sakon Nakhon, 47000, Thailand*
[f] *Center for Research and Development of Herbal Health Products, Khon Kaen University, Khon Kaen, 40002, Thailand*

ARTICLE INFO

Keywords:
Multi-mode of action
Butyrylcholine esterase
Amyloid beta
Neuroprotection
Molecular docking
Structure-activity relationship
Drug-likeness properties
ADMET

ABSTRACT

Alzheimer's disease (AD) is a neurodegenerative disorder characterized by cognitive impairment and neuronal death. Fifteen flavonoids from *Millettia brandisiana* were evaluated for the multifunctional effect against AD pathogenesis, including butyrylcholine esterase (BuChE) inhibition, anti-amyloid beta (Aβ) aggregation and neuroprotection against hydrogen peroxide (H_2O_2) toxicity in differentiated human neuroblastoma SH-SY5Y cell. To understand the mechanism and structure-activity relationship, binding interactions between flavonoids and the BuChE and Aβ were investigated *in silico*. Furthermore, drug-likeness properties and ADMET parameters were evaluated *in silico* using SwissADME and pKCSM tools. All flavonoids exhibit a good drug-likeness profile. Six flavonoids have potency in BuChE inhibition, and four flavonoids show potency in anti-Aβ aggregation. Flavonoids with the 6″,6″-dimethylchromeno- [2″,3″:7,8]-flavone structure show a favorable multifunctional effect. *In silico* analysis showed that flavonoids can bind in various positions to the catalytic triad, anionic site, and acyl pocket. In $A\beta_{1\text{-}42}$, potential flavonoids can attach to the central hydrophobic region and the C terminal hydrophobic and interfere with Aβ interchain hydrogen binding. When compared together, it can inhibit multifunctional action with a favorable ADMET parameter and drug-likeness profile. In addition, candidine can prevent neuronal damage in differentiated SH-SY5Y neuroblastoma cells induced by H_2O_2 in a dose-dependent manner.

1. Introduction

Alzheimer's disease (AD) is a neurodegenerative disorder characterized by cognitive and memory impairment and neuronal death

* Corresponding author. Faculty of Pharmaceutical Sciences, Khon Kaen University, Khon Kaen, 40002, Thailand.
E-mail addresses: puguh.arsito@gmail.com (P.N. Arsito), porntip.w@ubu.ac.th (P. Waiwut), chayen@kku.ac.th (C. Yenjai), supakorn.a@snru.ac.th (S. Arthan), oramon@kku.ac.th (O. Monthakantirat), nnatsa@kku.ac.th (N. Nualkaew), ppitcha.t@gmail.com (P. Takomthong), chaboo@kku.ac.th (C. Boonyarat).

https://doi.org/10.1016/j.heliyon.2023.e21894
Received 10 April 2023; Received in revised form 7 July 2023; Accepted 31 October 2023
Available online 8 November 2023

[1]. AD has several pathophysiological hypotheses, including amyloid beta cascade, neurofibrillary tangle generation, cholinergic nerve damage, neuroinflammation, and oxidative stress [2].

Based on the amyloid beta cascade, AD is characterized by the accumulation of amyloid-beta (Aβ) peptides in the brain. Amyloid precursor protein (APP) is a protein that modulates cell growth, motility, neurite growth, and cell survival. APP is first cleaved in the amyloidogenic pathway by β-secretase to form a dissolved protein (sAPPβ) and C-terminal membrane-bound fragments (βAPP-CTF). Subsequent cleavage of the βAPP-CTF fragment by γ-secretase includes the Aβ peptide [3]. Aβ monomer then aggregates into larger neurotoxic amyloid plaques [4]. In addition, oxidative stress has been linked to the etiology of AD since it stimulates Aβ production and contributes to Aβ neurotoxicity. The subsequent proteolysis of APP is carried out by β-secretase and γ-secretase, producing Aβ, which causes neurotoxicity [5].

Dysfunction of the cholinergic system also plays a role in AD occurrence. Thus, the therapeutic strategy that can be used is to increase acetylcholine (ACh) levels [6]. ACh can be hydrolyzed by acetylcholine esterase (AChE) and butyrylcholine esterase (BuChE) [7]. Under normal physiological conditions, ACh is hydrolyzed more by AChE than BuChE. However, in the development of late AD, AChE levels drop to 55–67 %, while BuChE levels rise to 120 %. Thus, a strategy to inhibit BuChE is an essential therapeutic option [8,9]. AChE and BuChE consist of four main sites, namely peripheral anionic site (PAS), anionic site (AS), acyl pocket (AP), and catalytic triad (CT). Catalytic triads of human AChE (hAChE) consist of three critical amino acids: Ser203, His447, and Glu334. In contrast, human BuChE (hBuChE) consists of Ser198, His438, and Glu325 [10,11]. In addition, AChE and BuChE have amino acid sequence similarity of 65 % [12].

The medications used to treat AD can only briefly relieve its symptoms; no medication can stop or reverse the illness's underlying progression. The most direct source of symptoms in AD is thought to be the loss of neurons and synapses in the brain. The FDA has only authorized six drugs to treat AD clinically [13]. AD drug development is currently focused on single targets, whereas the mechanism of AD is multifactorial. Intervention at multiple pathways is required for complicated illnesses like Alzheimer's disease [14].

Flavonoids have been extensively studied for various medical applications, and many of them were shown to display advantageous neuroprotective properties associated with multitarget mechanisms of action [15], such as catechol [16], biflavonoid [17], and epigallocatechin gallate (EGCG) [18]. Here we evaluated the potency of flavonoids from *Millettia brandisiana*. Many studies have reported their use as a traditional medicine to treat infected wounds, skin disorders, cough, rheumatoid pain, ulcer, menstrual disorder, inflammation, bronchitis, toothache, muscle ache, tuberculosis, hepatitis, and bruises [19]. *Millettia brandisiana* also has been studied for several activities, such as anticancer [20] and antioxidant [21].

In this study, fifteen flavonoids from *Millettia brandisiana* (Fig. 1.) were evaluated for drug-likeness properties by using the Swiss-ADME software. Furthermore, the pharmacological activity associated with AD was assessed using in vitro methods of inhibition of AB aggregation and inhibition of the BuChE. To understand the molecular mechanism of AB aggregation and inhibition BuChE, this study

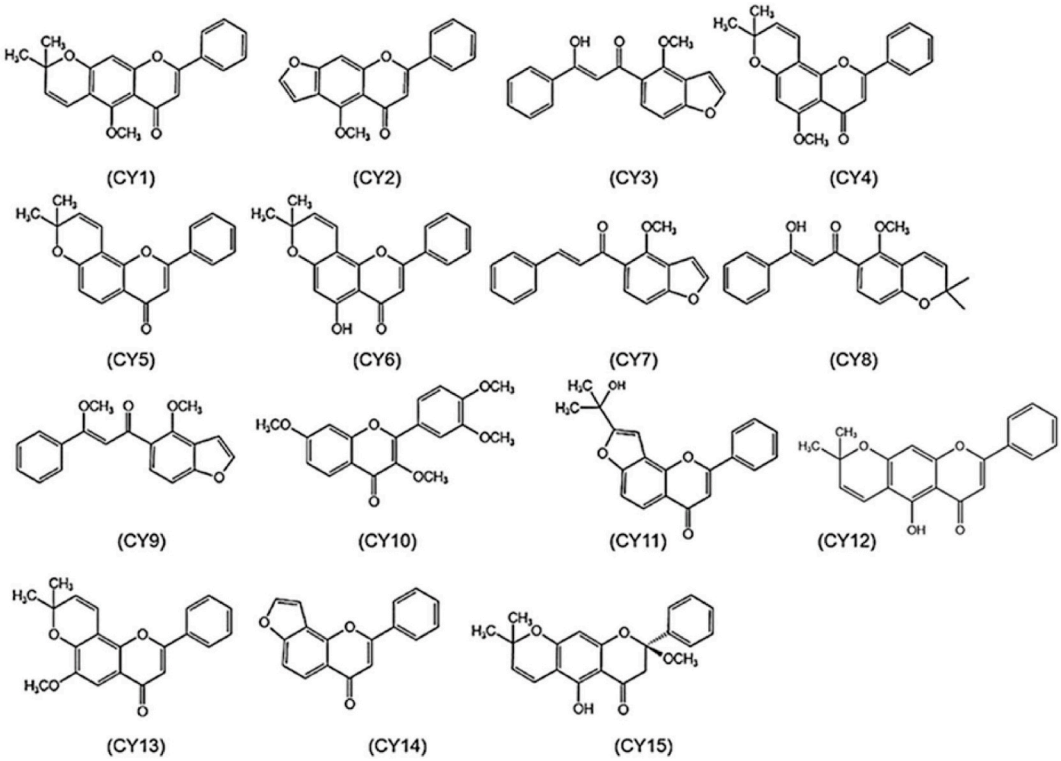

Fig. 1. Structure of flavonoid derivatives from *Millettia brandisiana*.

also investigated the mechanism of the inhibition by using *in silico* method (molecular docking and molecular dynamic). In addition, to confirm neuroprotection activity, fifteen flavonoids were also evaluated using a neuronal cell culture model induced by H_2O_2 cell damage. Finally, predictions of pharmacokinetic parameters and toxicity of fifteen flavonoids were analyzed *in silico* using pKCSM software.

2. Results

2.1. In silico prediction of the drug-likeness properties

The features of drug-likeness are essential prerequisites for developing rational anti-AD drugs. The physicochemical properties of the compounds have been evaluated *in silico*. The results are shown in Table 1. As can be seen, the compounds obey Lipinski's rule of five, indicating their drug-likeness properties.

2.2. In vitro BuChE inhibitory activity

The BuChE inhibitory activity of flavonoids was investigated using the Elmann spectrophotometric method, and donepezil was used as a positive control. The potential activity of flavonoids is known by comparing the IC_{50} value (concentration that can inhibit 50 % activity of BuChE). The result of BuChE inhibition is shown in Table 2.

2.3. In silico molecular docking and molecular dynamic simulation of BuChE inhibition

To determine the mechanism of BuChE inhibition, a molecular docking method was used. This method can determine the position of the compound when it binds to BuChE. The standard used in this molecular docking is donepezil, according to its in vitro test. The interaction profile of flavonoid compounds on the active site of BuChE can be seen in Table 3, while the binding interaction results can be seen in Fig. 2. From the simulation results, all tested flavonoid compounds and donepezil can be bound to AS, AP, and CT. However, only donepezil, CY9, and CY15 have additional binding to the PAS site.

Furthermore, the top four high scores IC_{50} of CY in BuChE inhibition were submitted to MD simulation tests using Open MM software to evaluate their binding stability during 50 ns simulation time. The PDB file of BuChE and the best ligand pose were obtained from the previous molecular docking step. The protein-ligand complex's stability throughout simulation is ultimately determined by the RMSD, which is calculated as the structure of a protein or protein-ligand complex's divergence from its original posture. Here, we describe the behavior of the RMSD of BuChE alone or in complex with CY1, CY5, CY12, and CY13 throughout a molecular dynamics simulation under physiological circumstances (Fig. 3). To determine how stable a protein-ligand combination is throughout the simulation, the variation in a protein or protein-ligand complex structure from its initial posture is measured as RMSD.

Following that, we computed RMSF (Root Mean Square Fluctuation) values in order to explore the structural flexibility of the atoms that make up the proteins backbone in both the complex and Apo forms. Here, Fig. 4 depicts the behavior of the RMSD of BuChE alone or in complex with CY1, CY5, CY12, and CY13 throughout a molecular dynamics simulation under physiological circumstances (Fig. 4).

The relationship between the ligand radius of gyration (Rg) and simulation duration shows how the ligand behaves inside the enzyme's binding pocket. The Rg values indicate the RMSD of an atom's breadth from the common mass center. The Rg can also ascertain whether the complex stays folded throughout the MD simulation. The fluctuation in Rg of Apo BuChE and BuChE bound to different substances (CY1, CY5, CY12, and CY13) as a function of simulation time is shown in Fig. 5.

To assess protein-ligand stability in the presence of a solvent, we used the molecular mechanics generalized Born surface area (MM/

Table 1
Physicochemical properties prediction of flavonoids (SwissADME program).

Compound	Molecular weight (g/mol)	H-bond acceptors	H-bond donor	Rotatable bonds	Polar surface area (A^2)	ClogP	Lipinski & Veber rule
CY1	334.37	4	0	2	48.67	3.9	yes
CY2	292.29	4	0	2	52.58	3.36	yes
CY3	294.3	4	1	4	59.67	3.26	yes
CY4	284.31	4	0	2	48.67	2.48	yes
CY5	254.28	3	0	1	39.44	2.46	yes
CY6	320.34	4	1	1	59.67	3.58	yes
CY7	278.3	3	0	4	39.44	3.59	yes
CY8	336.38	4	1	4	55.76	3.81	yes
CY9	308.33	4	0	5	48.67	3.46	yes
CY10	342.34	6	0	5	67.13	3.08	yes
CY11	320.34	4	1	2	63.58	3.49	yes
CY12	320.34	4	1	1	59.67	3.72	yes
CY13	336.38	4	0	2	48.67	3.21	yes
CY14	262.26	3	0	1	43.35	3.41	yes
CY15	352.38	5	1	2	64.99	3.53	yes

Table 2
The IC_{50} (μM) of BuChE and Aβ aggregation inhibitory activities of flavonoids.

Compound	BuChE assay (IC_{50}, μM)	Aβ aggregation (IC_{50}, μM)
CY1	$4.95 \pm 0.19^{b,c}$	>200
CY2	81.95 ± 1.30^{f}	195.3 ± 3.2^{f}
CY3	102.21 ± 1.27^{g}	>200
CY4	$8,27 \pm 0.52^{c,d}$	108.7 ± 1.7^{c}
CY5	$4.04 \pm 0.23^{a,b}$	$169.9 \pm 2.7^{d,e}$
CY6	$7.60 \pm 0.24^{b,c,d}$	70.3 ± 2.8^{b}
CY7	58.81 ± 2.28^{e}	>200
CY8	>200	>200
CY9	107.97 ± 1.30^{h}	>200
CY10	>200	155.0 ± 6.2^{d}
CY11	>200	>200
CY12	$4.01 \pm 0.61^{a,b}$	$180.2 \pm 16.4^{e,f}$
CY13	1.16 ± 0.27^{a}	85.1 ± 3.1^{b}
CY14	$174.65 \pm 2,19^{i}$	105.56 ± 3.1^{c}
CY15	>200	>200
Donepezil	9.35 ± 0.11^{d}	Not detected
Curcumin	Not detected	4.8 ± 0.12^{a}

nd = not detected. ^{a,b,c,d,e,f,g,h,i} Means in a row with different superscript letters are statistically analyzed by one-way ANOVA ($p < 0.05$).

GBSA) method to calculate binding free energy. This study estimated the MM/GBSA of the BuChE and CY compound, and the findings are shown in Table 4. 10.998 complex frames from 50 ns MD simulations were used for calculations. ΔG binding was calculated using Eq. (1).

$$\Delta G_{binding} = \Delta G_{complex} - (\Delta G_{protein} + \Delta G_{ligand}) \ldots\ldots\ldots\ldots\ldots \quad \text{(Eq. 1)}$$

Each free energy term in Eq. (1) was computed as a sum of the gas phase molecular mechanical energy (ΔE gas), the solvation free energy (ΔG solvation)

$$\Delta G_{binding} = \Delta E_{gas} + \Delta G_{solvation} \ldots\ldots\ldots\ldots\ldots \quad \text{(Eq. 2)}$$

ΔE gas can be divided into contributions from the van der Waals energy (ΔE_{vdW}), electrostatic energy (ΔE_{ele}),

$$\Delta E_{gas} = \Delta E_{vdW} + \Delta E_{ele} \ldots\ldots\ldots\ldots\ldots \quad \text{(Eq. 3)}$$

The solvation-free energy, ΔG solvation, estimated using continuum solvent methods, can be partitioned into two parts the polar contribution (ΔG_{P_solv}) and the nonpolar contribution (ΔG_{NP_solv}).

$$\Delta G_{solvation} = \Delta G_{P\_solv} + \Delta G_{NP\_solv} \ldots\ldots\ldots\ldots\ldots \quad \text{(Eq. 4)}$$

The principal component analysis (PCA) method was used to examine the conformational changes in all four complexes throughout the simulations. The PCA was plotted using the two eigenvectors as input to compare the most likely motions. Each dot in the plot represents one of the four complexes, and the actions indicate their conformational changes. The portrayal of the periodic transitions between conformations in green color gradients stands out. The result of PCA can be seen in Fig. 6.

2.4. Amyloid aggregation inhibitory activity

To determine the inhibitory effect of $A\beta_{1-42}$ aggregations by flavonoids, the ThT fluorescence method was used. The compound used as a positive standard was curcumin. The observations show that several flavonoids have an inhibitory effect on the aggregation of $A\beta_{1-42}$. IC_{50} values can be seen in Table 2. In addition, the superposition of docked orientations of all flavonoids from *Millettia brandisiana* on the amyloid beta can be seen in Fig. 7. At the same time, the molecular docking simulation of flavonoid to the Aβ can be seen in Fig. 8.

2.5. Neuroprotective effect against H_2O_2-induced cell death

To determine the neuroprotective activity against oxidative stress, all flavonoids were screened for their potential toxicity on differentiated SH-SY5Y cells for 2 h. The results of the toxicity test can be seen in Table 5. From the toxicity test results, it is known that some flavonoids at a concentration of 100 μM showed toxic effects. Still, at a dose of 10 μM, all flavonoids did not show toxic effects so that it can be determined for a further neuroprotective test to use a dose of 10 μM.

All flavonoids at a concentration of 10 μM were tested for their neuroprotective activity against 250 μM of H_2O_2 induction for 3 h. Curcumin at a dose of 10 μM also used as a positive standard. The results of the initial screening of neuroprotective activity can be seen in Fig. 9. All flavonoids showed neuroprotective activity. Furthermore, CY6 flavonoid compounds have multifunctional effects inhibiting Aβ aggregation, BuChE inhibition, and neuroprotective potential. While the CY9 compound had no potential effect on

Table 3
Interaction of flavonoid of *Millettia brandisiana* to the active site of BuChE.

Compound	Peripheral anionic site (PAS)		Anionic site (AS)		Acyl pocket (AP)					Catalytic triad (CT)		
	Tyr 332	Asp 70	Trp 82	Ala 328	Trp 231	Leu 286	Val 288	Phe 329	Phe 398	Ser 198	His 438	Glu 325
Group A CY4			π-π T shape	π alkyl	π-π T shape	π-alkyl		π-π T shape		πdonorH bond	π cation	
CY5			π-π T shape	π alkyl	π-π T shape	π-alkyl		π-π T shape		πdonorH bond	πcation	
CY6			π sigma	π alkyl		π alkyl					π cation	
CY13			π sigma	π alkyl	π-alkyl			π alkyl		van der Waals	π cation	
Group B CY1			sigma	π alkyl	π-π T shape	π sigma		π-π T shape	C–H bond	π cation		
CY12			π π T shape	π alkyl	π sigma	π alkyl	π alkyl			π alkyl	van der Waals	π cation
CY15		C–H bond	π-π T shape	π alkyl	π sigma	π alkyl		π π T shape		π alkyl	H bond	
Group C CY2					π-π T shape	π-alkyl	π alkyl	π-π T shape	H-bond	H bond		
CY10			π sigma	π alkyl		π-alkyl		π-π T shape	H bond	H bond		
CY11			H bond	π alkyl							H bond	
CY14			C–H bond	π alkyl							π cation	
Group D CY3				π alkyl	π-π T shape	π-alkyl		π-π T shape	C–H bond	π cation		
CY7			π-π stacked	π alkyl						H bond	H bond	
CY8			H bond	π alkyl	π-π T shape	π alkyl						
CY9	π alkyl		H bond	C H bond	π-π T shape	π-alkyl		π-π T shape	H bond	H bond		
Donepezil	pi sigma		Van der Waals.	pi alkyl				pi alkyl			pi alkyl	

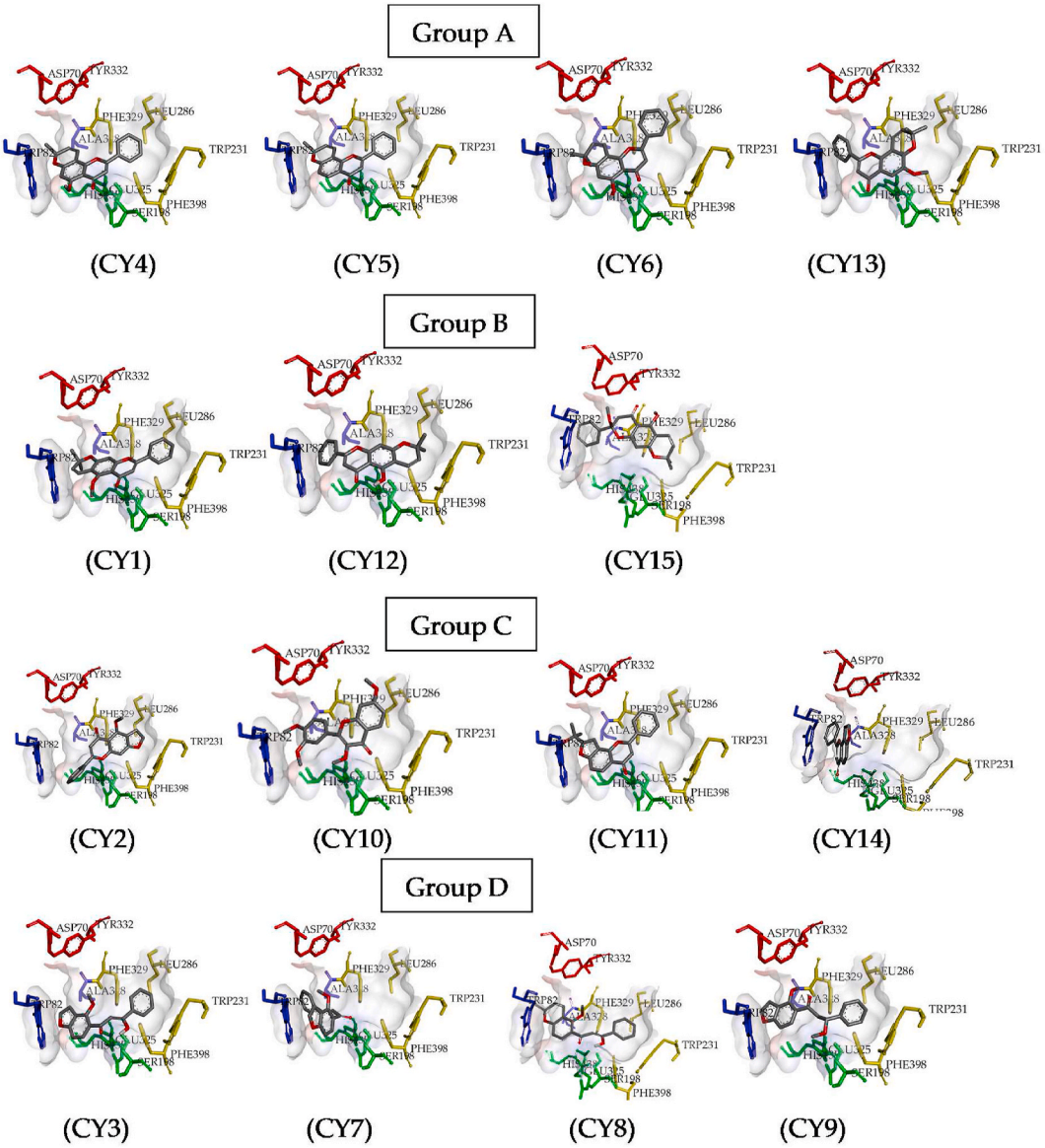

Fig. 2. Binding interactions of flavonoid derivatives. The binding sites are coded with different colors (PAS; red, AS; blue, AP; yellow, CT; green). 5-Methoxy-6″,6″-dimethylchromeno-[2″,3″:7,6]-flavone (CY1), pinnatin (CY2), pongamol (CY3), isopongaflavone (CY4), 6″,6″-dimethylchromeno-[2″,3″:7,8]-flavone (CY5), candidine (CY6), ovalitenin A (CY7), 2′-methoxy-6″,6″-dimethylchromeno-[2″,3″:4′,3′]-β-hydroxy chalcone (CY8), O-methylpongamol (CY9), 3,3′,4′,7-tetra-O-methyl fisetin (CY10), brandisianone B (CY11), 5-hydroxy-6″,6″-dimethylchromeno-[2″,3″:7,6]-flavone (CY12), 6-methoxy-6″,6″-dimethylchromeno-[2″,3″:7,8]flavone (CY13), Lanceolatin B (CY14), brandisianone F (CY15).

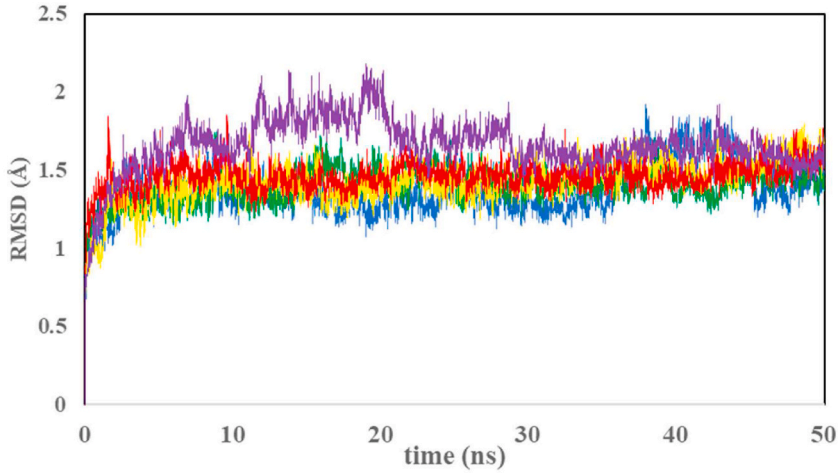

Fig. 3. The behavior of Root Mean Square Deviation (RMSD) of protein Cα atoms during 50 ns simulation. Apo BuChE (blue), BuChE + CY13 (green), BuChE + CY12 (yellow), BuChE + CY5(red), BuChE + CY1 (purple).

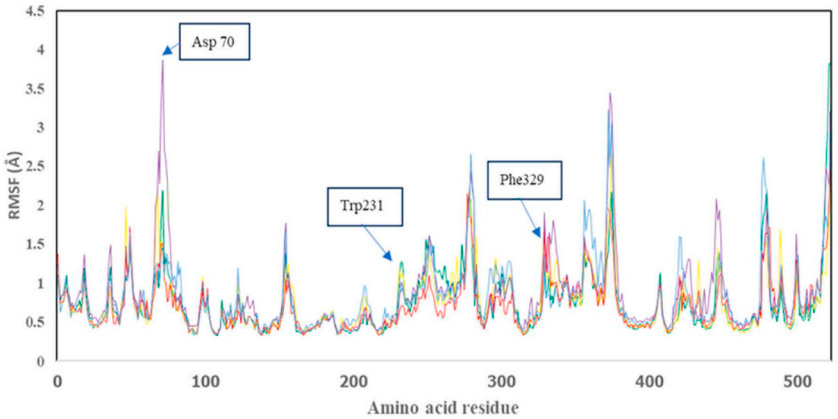

Fig. 4. Average Root mean square fluctuation (RMSF) values of Apo BuChE (blue), BuChE + CY13 (green), BuChE + CY12 (yellow), BuChE + CY5 (red), BuChE + CY1 (purple).

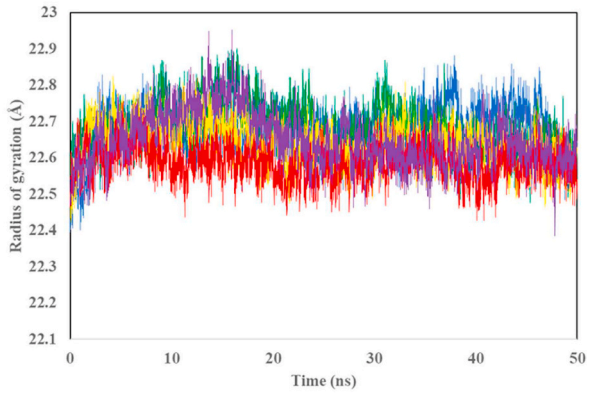

Fig. 5. Radius of gyration (Rg) values of Apo BuChE (blue), BuChE + CY13 (green), BuChE + CY12 (yellow), BuChE + CY5(red), BuChE + CY1 (purple).

Table 4
The binding free energy (kcal/mol) components for the BuChE complexes with CY1, CY5, CY12, and CY13 were determined using the MM/GBSA method.

Inhibitor	ΔE_{vdW}	ΔE_{Ele}	ΔG_{P_solv}	ΔG_{NP_solv}	ΔG_{gas}	ΔG_{solv}	ΔG_{total}
CY1	−36.357 ± 5.7	−1.696 ± 3.6	16.74 ± 5.0	−4.014 ± 0.7	−38.054 ± 6.0	12.726 ± 4.7	−25.327 ± 5.3
CY5	−39.234 ± 2.0	−1.461 ± 1.0	18.207 ± 0.9	−4.98 ± 0.1	−40.696 ± 2.1	13.226 ± 0.9	−27.469 ± 1.9
CY12	−36.275 ± 2.1	−4.243 ± 5.8	19.419 ± 4.1	−4.448 ± 0.2	−40.518 ± 5.7	14.971 ± 4.0	−25.547 ± 2.3
CY13	−40.092 ± 1.8	−2.322 ± 2.4	19.641 ± 2.3	−5.142 ± 0.2	−42.414 ± 2.9	14.499 ± 2.2	−27.914 ± 1.7

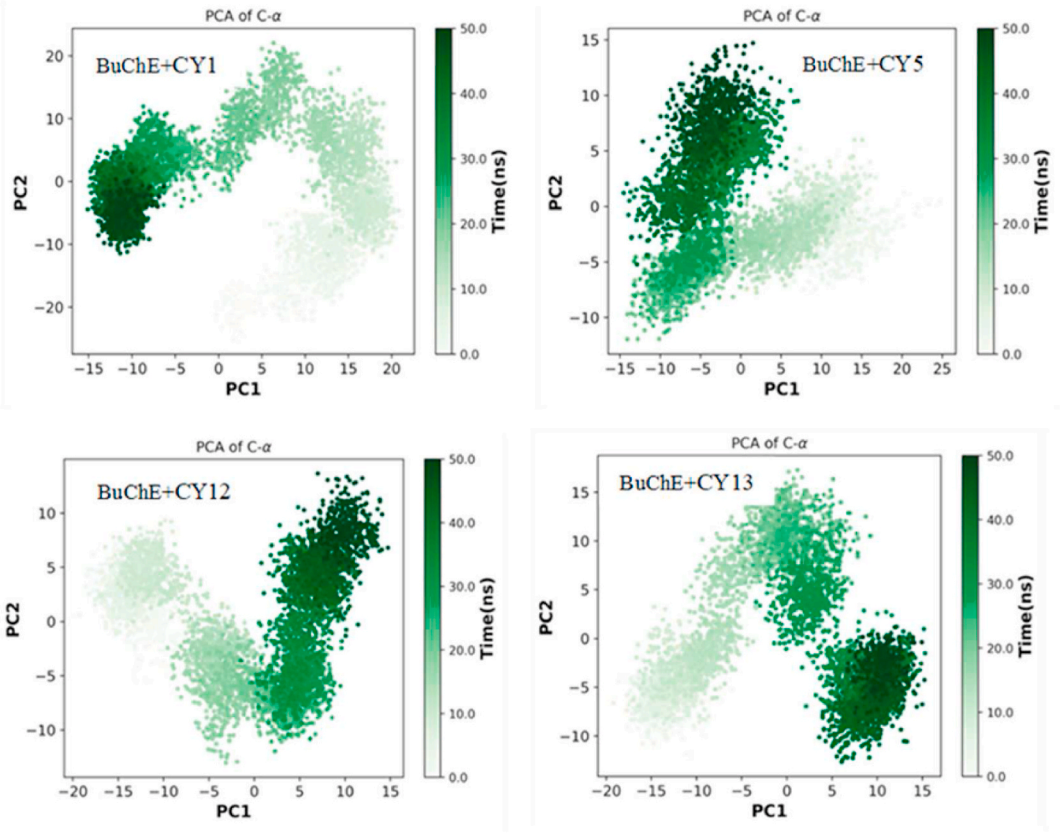

Fig. 6. Principal component analysis of BuChE complex with CY1, CY5, CY12, and CY13.

inhibiting Aβ and BuChE aggregation, the potential for a neuroprotective effect was the highest. Therefore, the CY6 and CY9 compounds were further investigated for their neuroprotective potential at various doses.

The dose variation neuroprotective test used concentrations of 0.1 μM, 1 μM, and 10 μM. CY 6 and CY 9 compounds were added to differentiated H_2O_2 cells for 2 h, and then neurotoxicity was induced using H_2O_2 at a dose of 250 μM for 3 h. The results of this neuroprotective test can be seen in Fig. 10. From the test results, neurotoxic induction using H_2O_2 can reduce cell viability by up to 40 %. However, in the treatment group using CY6 and CY 9 compounds, there was an increase in cell viability. This suggests that CY6 and CY9 have potential neuroprotective effects.

2.6. In silico drug ADMET evaluation

The drug's pharmacokinetic profile is essential for rationally developing anti-AD drugs. Therefore, the test compounds' ADMET (absorption, distribution, metabolism, excretion, and toxicity) have been evaluated *in silico*. The results are shown in Table 6.

3. Discussion

In the drug discovery process, the steps that need to be considered are the physicochemical properties and the profile of ADMET. In this study, SwissADME software was used to predict drug likeness. The purpose of this virtual screening is to avoid failures in drug development. New drug candidate molecules are reported to fail up to 95 % in drug development. 50 % of the causes of this failure are

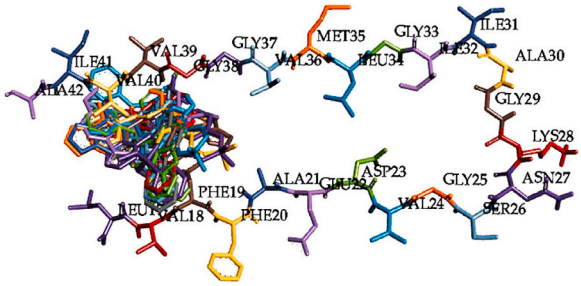

Fig. 7. Superposition of docked orientations of all flavonoids from *Millettia brandisiana* on amyloid beta (PDB code: 2BEG).

due to physicochemical properties and ADMET that does not meet the properties requirements. For drug-likeness prediction, data for the physicochemical properties of flavonoid compounds can be seen in Table 1. From the screening results, all 15 molecules meet the Lipinski rule [22] with no violation. The molecular weight of the largest compound was 352.38 (CY15) and was still below 500. In the H-bond acceptor and donor parameters, it was seen that all combinations still met the requirements of less than 10 and 5, respectively. Furthermore, the Veber rule parameter predicts the total polar surface area (TPSA) and the total rotatable area. From this parameter, it can be known whether the compound is still in the range of oral bioavailability. Based on the prediction, the compound appears to meet Veber's rule [23]. Therefore, the results indicated that all flavonoid compounds from *Millettia brandisiana* can potentially be developed into new drug molecules.

Several studies reported that flavone and chalcone bound to BuChE active sites with various positions in the CT and PAS with their potential activity [24,25]. These reports support our result that flavonoids from *M. brandisiana* show potential BuChE inhibition with the lowest IC_{50} value CY13 (1.16 μM). To understand the relationship between structure and inhibitory activity of BuChE, flavonoids were grouped into four groups, namely group A (6″,6″-dimethylchromeno-[2″,3″:7,8] flavone), B (6″,6″ dimethylchromeno-[2″,3″:7, 6]-flavone), C (furanoflavone derivatives) and D (furanochalcone derivative). In group A, CY5 has an IC_{50} value of 4.04 μM. At CY6 Substitution of the hydroxyl group at C number 5 resulted in an increase in IC_{50} to 7.6 M, as well as the substitution of a methoxy group at C number 5 (CY4), the IC_{50} value increased to 8.27 M. Interestingly, the change in methoxy substitution at C number 6 (CY13) made the IC_{50} value lower to 1.16 M. There are four essential parts of the BuChE active site, namely peripheral anionic site/PAS (Tyr332, Asp70), anionic site/AS (Trp82, Ala328), acyl pocket/AP (Trp231, leu286, Val288, Phe329, Phe398), and catalytic triad/CT (Ser198, His 438, Glu325) with a total gorge wide area of 500 $Å^3$ [11]. The docking simulation shows that all group A flavonoids can be bound to the AS, AP, and CT sites with varying orientations. At CY5 and CY4, rings A and C of flavones are attached to the CT site (His438, ser 198), ring B is bound to the AP site (Trp231, Phe329, Leu286), the dimethylchromen ring is attached to AS (Trp82 & Ala 328). Interestingly, the change in methoxy substitution at C number 6 (CY13) changes the orientation of the bond. At CY13, ring B becomes bound to AS (Trp82 & Ala328), rings A and C bind to the CT site, while the dimethychromene ring becomes attached to AP (Trp 231 & Phe 329). This change in the orientation of CY13 makes the ring C binding distance to CT His438 closer (2.77 & 3.92 A) when compared to CY5 and CY4. This makes the potency of CY13 even stronger. It is known that methoxy substitution at group number 6 can increase potency, while methoxy and hydroxy substitution at C5 will decrease potency.

Further comparison can be seen between group A and group B. The difference in the position of the dimethyl chromene group affects the potential for inhibitory activity. CY12 has a stronger potency than CY6. When viewed in the docking simulation, it appears that CY12 has more bonds than CY6. On the AP, CY12 has four bonds (Trp231, Leu286, Val 288, Phe398) residues, while CY6 only has one bond in Leu 286. In addition, CY12 has three bonds in CT, while CY6 only has one. A similar phenomenon also occurs in CY1, which has a stronger potency than CY4. The number of amino acids bound to CY1 and CY4 is the same, but at CY1, the distance between the C ring of flavones to the catalytic residue of His438 is closer (3.34 A) when compared to CY4 (4.58 A). This shows that the 6″,6″-dimethylchromeno-[2″,3″:7,6] position of flavones has a stronger potency than the 6″,6″-dimethylchromeno-[2″,3″:7,8] position of flavones.

The next is the comparison between groups B and C. In the CY1 and CY2, replacing the dimethylchromeno flavone group with Furanoflavone can reduce the inhibitory potential of BuChE, and the IC_{50} value drops from 4.95 μM to 81.95 μM. CY2 can only bind to the CT and AP when confirmed using the docking simulation, while CY1 can attach to the CT, AP, and CS. A change in the position of methoxy at carbon number 2 and hydroxy in carbon number 5 (CY15) resulted in a decrease in potency compared to CY1. In group B, this indicates that the methoxy substitution at C number 5 influences potency. The following comparison is in group D (furanochalcone). In general, the potency of Furanochalcone is lower than that of dimethylchromeno flavone. The strongest potency of furanochalchone derivatives is CY7 (IC_{50} 58.81 M). When CY7 was compared with CY3(IC_{50} 102.21 M), it was seen that the hydroxy substitution at C number 7 seemed to decrease potency. The same thing also happened to substitute methoxy at C number 7; the IC50 value increased to 107.97 μM. The docking simulation also shows that CY7 has no hydroxy or methoxy substitution at C number 7, resulting in a relatively small molecule that can enter the catalytic gorge (His438, Ser198) and form hydrogen bonds with the CY7 ketone group. Meanwhile, CY9, substituting with methoxy, makes its structure bulkier and bound from the PAS, AS, and AP to the CT.

In MD simulations, graph analyses allow for understanding a protein's progressively increasing RMSD values prior to stabilization. As the enzyme complexed with the ligand (CY5, CY12, or CY13), its stability phase was from 15 ns, with average RMSD values of 1.45 $\pm$ 0.09 Å, 1.42 $\pm$ 0.13 Å, and 1.39 $\pm$ 0.10 Å, respectively. The stability phase of APO BuChE (enzyme without the ligand) was observed

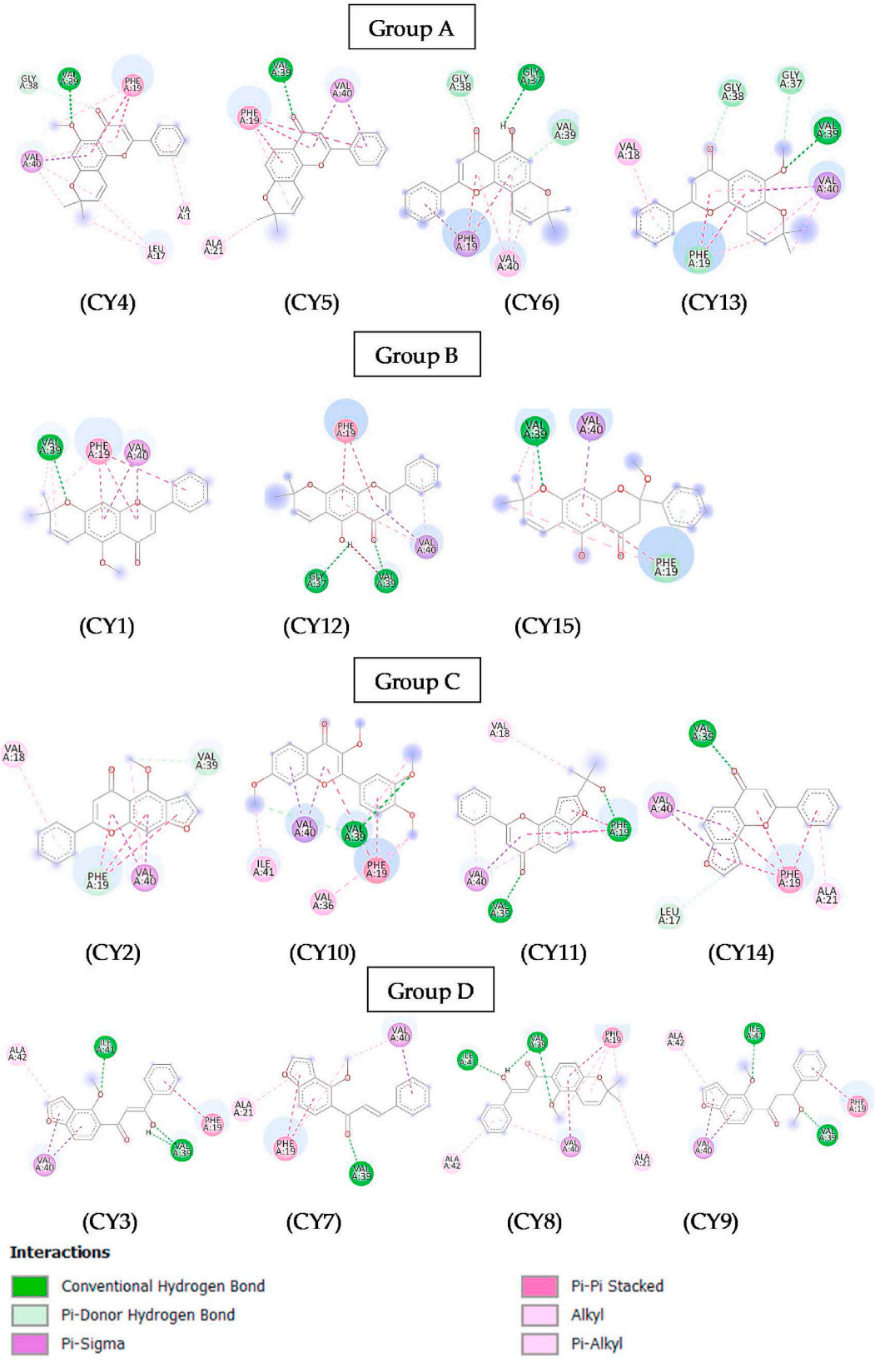

(caption on next page)

Fig. 8. Binding interactions of flavonoid derivatives to the amyloid beta. 5-methoxy-6″,6″-dimethylchromeno-[2″,3″:7,6]-flavone (CY1), pinnatin (CY2), pongamol (CY3), isopongaflavone (CY4), 6″,6″-dimethylchromeno-[2″,3″:7,8]-flavone (CY5), candidine (CY6), ovalitenin A (CY7), 2′-methoxy-6″,6″-dimethylchromeno-[2″,3″:4′,3′]-β-hydroxychalcone (CY8), O-methylpongamol (CY9), 3,3′,4′,7-tetra-O-methyl fisetin (CY10), brandisianone B (CY11), 5-hydroxy-6″,6″-dimethylchromeno-[2″,3″:7,6]-flavone (CY12), 6-methoxy-6″,6″-dimethylchromeno-[2″,3″:7,8]flavone (CY13), Lanceolatin B (CY14), brandisianone F (CY15).

Table 5
Effects of flavonoids and curcumin on cell viability of differentiated SH-SY5Y cells. The values are reported as mean ± SD (n = 5). One-way ANOVA, *p < 0.05 versus the control group.

Group	Cell viability (% control)				
	100 μM	10 μM	1 μM	0.1 μM	Control
CY1	81.5 ± 1.3	95.3 ± 1.5	97.1 ± 1.2	97.1 ± 1.7	100 ± 1.3
CY2	68.5 ± 2.2 *	96.1 ± 4.3	99.3 ± 4.7	96.7 ± 3.1	100 ± 1.3
CY3	103.1 ± 4.0	104.3 ± 3.8	103.6 ± 1.1	103.3 ± 1.4	100 ± 1.8
CY4	98.8 ± 3.7	101.6 ± 1.3	103.3 ± 2.7	101.6 ± 2.6	100 ± 0.5
CY5	79.3 ± 3.0 *	98.4 ± 3.4	97.4 ± 3.5	97.1 ± 3.8	100 ± 2.3
CY6	83.4 ± 1.1 *	92.6 ± 1.2	102.7 ± 1.8	105.1 ± 2.0	100 ± 2.3
CY7	15.9 ± 3.0 *	103.2 ± 3.4	105.1 ± 3.5	102.5 ± 4.2	100 ± 4.5
CY8	82.3 ± 2.5 *	101.2 ± 1.4	100.2 ± 2.5	102.1 ± 1.2	100 ± 4.5
CY9	98.5 ± 4.1	98.4 ± 3.1	100.8 ± 11.1	102.1 ± 4.6	100 ± 4.1
CY10	38.2 ± 1.9 *	99.6 ± 3.3	102.4 ± 4.1	103.2 ± 4.0	100 ± 6.6
CY11	85.4 ± 1.1 *	99.2 ± 4.1	98.9 ± 4.9	100.2 ± 2.5	100 ± 3.1
CY12	86.9 ± 5.4 *	100.3 ± 6.3	100.4 ± 4.1	103.3 ± 3.6	100 ± 4.06
CY13	75.3 ± 2.3*	98.5 ± 2.1	99.1 ± 3.2	101.4 ± 3.1	100 ± 2.5
CY14	72.4 ± 3.4*	97.4 ± 3.2	100.1 ± 2.6	102.4 ± 1.3	100 ± 3.6
CY15	76.3 ± 4.7 *	99.7 ± 3.5	99.9 ± 4.6	99.2 ± 3.6	100 ± 6.6
Curcumin	79.1 ± 3.6*	100.5 ± 7.7	100.4 ± 4.6	104.1 ± 3.2	100 ± 4.8

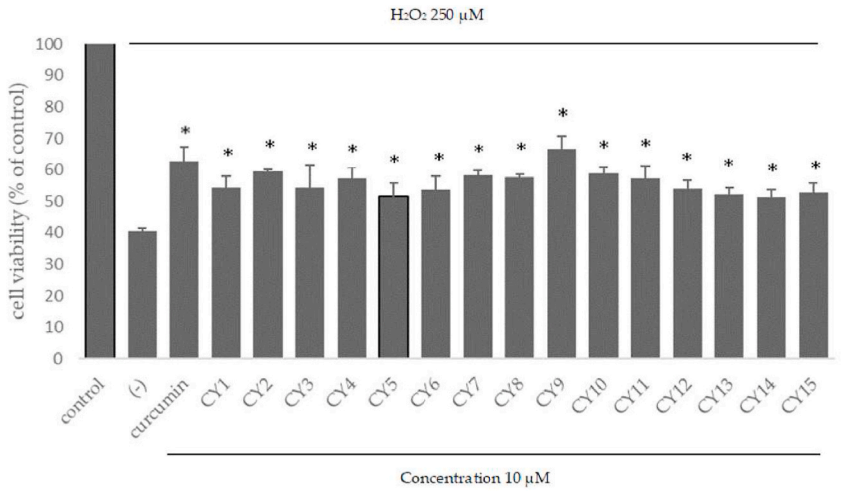

Fig. 9. Effects of flavonoids on H_2O_2 induced cell death in differentiated SH-SY5Y cells. Curcumin at 10 μM was used as a reference standard. The values are reported as mean ± SD (n = 5). One-way ANOVA, *p < 0.05 versus H_2O_2 treated group.

from 15 ns of simulation, with an average RMSD value of 1.36 ± 0.15 Å. Except for the CY1 complex, the stability phase was seen between 25 and 50 ns, with a mean RMSD value of 1.65 ± 0.02 Å; overall, RMSD less than 2.5 Å is regarded as acceptable when all system atoms are used for evaluation, given that equilibrium variation occurs because of the protein's inherent properties. Using the RMSD metric, which mathematically denotes minute variations in the enzyme patterns, the conformational changes in the AChE and BuChE structures relative to their original structures and the determination of the point at which the systems reached equilibrium were also examined.

The residues 476–482, 370–378, 277–282, and 66–75 in the C-terminal sections of Apo BuChe and the complex BuChE CY compound have been discovered to exhibit larger changes in protein RMSF measurements during simulations of molecular dynamics. The average RMSF values for apo BuChE and BuChE in the presence of CY1, CY5, CY12, and CY13 were, respectively, 0.803 Å, 0.859 Å, 0.706 Å, 0.749 Å, and 0.736 Å. These findings show that the RMSF of BuChE did not significantly change when the CY compound was present. The average values remained within the permitted range, indicating that the general structure of target proteins was

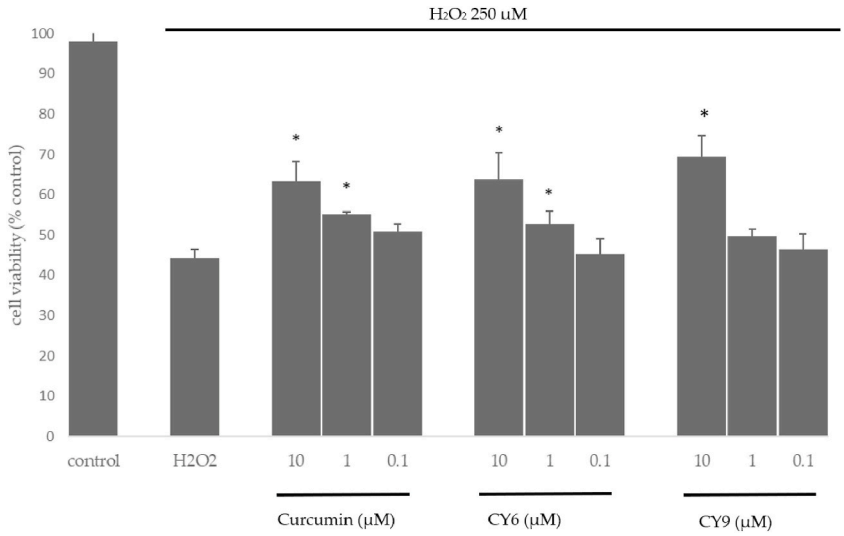

Fig. 10. Effects of CY6 and CY9 on H_2O_2-induced cell damage in differentiated SH-SY5Y cells. Curcumin was used as a reference standard. The values are reported as mean ± SD (n = 5). One-way ANOVA, *p < 0.05 versus H_2O_2 treated group.

conserved. Less fluctuating active site residue is the result of more stable and robust interactions between AChE and the CY molecule, as shown in Fig. 3's reduced RMSF values for the BuChE-CY complex. Two active sites that show the RMSF's variation are PAS (Asp70) and AP (Trp231, Phe 329). Compared to the other three BuChE complexes, the BuChE + CY1 complex has the highest IC_{50} and the most variable RMSF. Particularly at the AP location, the RMSF fluctuation of the BuChE + CY13 complex is somewhat low. This outcome aligns with in vitro data showing CY13 to have a low IC_{50} value. The BuChE + CY13 complex's decrease in RMSF values demonstrated that CY13 has a more potent and sustained inhibitory capacity than other compounds.

The fluctuation in Rg of Apo BuChE and BuChE bound to different substances (CY1, CY5, CY12, and CY13) as a function of simulation time is shown in Fig. 5. The results showed that several protein-ligand systems' Rg values fluctuated within an acceptable range during the simulation. Apo BuChE and BuChE in the presence of CY1, CY5, CY12, and CY13 Rg values were 22.67 ± 0.06 Å, 22.65 ± 0.07 Å, 22.58 ± 0.04 Å, 22.64 ± 0.05 Å, and 22.68 ± 0.06 Å, respectively,

The BuChE + CY13 complex, which is shown in Table 4, has the lowest G total energy (−27.914 ± 1.7 kcal/mol), followed by BuChE + CY5 (−27.469 ± 1.9 kcal/mol), BuChE + CY12 (−25.54 ± 2.3 kcal/mol), and BuChE + CY1 (−25.32 ± 5.3 kcal/mol). The main factor in creating a stable protein-ligand complex is van der Waals' energy (G_{vdW}) from the G gas. This outcome is consistent with in vitro data showing that the CY13 with the lowest point also has the lowest IC_{50} for inhibiting BuChE.

According to the PCA results, the structural movements in the complexes BuChE + CY1 and BuChE + CY5 were greater than those in the complexes BuChE + CY12 and BuChE + CY13. Less conformational change was seen in the short phase space (i.e., 15. to 12.5) when enzymes were inhibited by CY12 and CY13, indicating consistent and stable behavior. In contrast, CY1 and CY5 showed significant conformational changes during the MD simulations and achieved a variety of motion in phase space (i.e., 20 to 15) when used to inhibit enzymes.

The Aβ peptide is a key component of senile plaques and plays a role in neuronal and synaptic dysfunction as Alzheimer's disease progresses [26]. Aβ plaque dominantly consists of $Aβ_{1-40}$ and $Aβ_{1-42}$, which have highly distinct structural shapes [27,28]. $Aβ_{42}$'s C-terminus becomes more rigid, and residues 31–34 and 38–41 build a -hairpin that decreases C-terminal flexibility, which can explain how $Aβ_{42}$ is much more likely to occur in amyloids than $Aβ_{40}$ [4]. $Aβ_{42}$ peptide consists of unstructured residues (1-17) and β-turn-β fold residue (residues 18–42). There is also a β-turn region which consists of residues 17–21 and 29–35, which stabilize by a salt bridge connecting Asp 23 and Lys28 [29]. In addition, two molecular bindings exist between Phe19-Gly38 and Ala42-Met35, which can stabilize the beta-sheet structure. During the nucleation, the process occurs in the central hydrophobic region (residues 17–21) and C terminal hydrophobic (residues 39–42). Furthermore, hydrogen binding can occur between interchain interactions (Val18-Val39, Phe20-Gly37, Glu22-Met35, Asp23-leu34, Lys28-Val36, Val36-Ile41) [30]. Thus, the β turn region, C terminal hydrophobic, and central hydrophobic region are critical to starting Aβ fibril nucleation and formation. The potency of flavonoids to modulate the Aβ formation was studied in vitro using thioflavin T (ThT) fluorometric assay and docking simulation. From the results of the Aβ anti--aggregation test, it was seen that some flavonoids have potential activity; in group A (6″,6″-dimethylchromeno-[2″,3″:7,8] flavone derivatives, CY6 has the highest IC_{50} (70.3 μM). When CY6 is compared to CY5 (IC_{50} 169 μM), removing the hydroxyl group decreases the activity. Furthermore, comparing CY6, CY4 (IC_{50} 108.7 μM), and CY13 (IC_{50} 85 μM) showed the replacement of the hydroxyl group with the methoxy group in position C5 or C6 also appears to decrease the activity. However, if CY4 is compared to CY13, the methoxy group at position C6 seems advantageous for the intended action.

On confirmation using docking simulation, it was seen that all group A flavonoids could be bound to central hydrophobic sites (Phe 19) and C terminal hydrophobic (Val39 and Val40) with various bonding. In CY6, the hydroxy substituent can form hydrogen bonds with Gly 37, essential for AB interchain interactions. In addition, ring B also includes bonds with Val39, while the ketone group of CY6

Table 6
Prediction of ADMET parameters of flavonoids (pKCSM program).

Compound	CY1	CY2	CY3	CY4	CY5	CY6	CY7	CY8	CY9	CY10	CY11	CY12	CY13	CY14	CY15
Absorption															
Intestinal absorption (Human) (% Absorbed)	97.58	97.18	93.232	97.229	96.509	94.455	96.25	93.936	87.022	98.547	94.938	94.811	97.103	95.927	94.764
Distribution															
BBB permeability (log BB)	0.354	0.307	−0.089	0.122	0.396	0.081	0.213	−0.324	0.46	−0.482	0.265	0.316	0.409	0.524	0.011
CNS permeability (Log PS)	−1.483	−1.594	−1.877	−1.451	−1.398	−1.557	−1.382	−1.844	−1.341	−2.298	−1.53	−1.578	−1.466	−1.289	−1.956
Metabolism															
CYP3A4 substrate	Yes	Yes	Yes	Yes	Yes	Yes	Yes	Yes	No	Yes	Yes	Yes	Yes	Yes	Yes
CYP2D6 substrate	No	No	No	No	No	No	No	No	No	No	No	No	No	No	No
CYP3A4 inhibitor	Yes	Yes	No	No	Yes	Yes	No	Yes	No	No	Yes	Yes	No	Yes	No
CYP2D6 inhibitor	No	Yes	No	No	No	No	No	No	No	No	No	No	No	No	No
Excretion															
Total Clearance ((log ml/min/kg)	0.342	0.48	0.346	0.344	0.239	0.281	0.182	0.218	0.239	0.804	0.333	0.292	0.257	0.381	0.264
Renal OCT2 substrate	Yes	No	No	Yes	No	No	No	No	No	Yes	No	Yes	Yes	No	No
Toxicity															
Hepatotoxicity	No	No	No	No	Yes	No	No	No	No	No	Yes	No	Yes	No	Yes
AMES test	No	Yes	No	No	Yes	No	No	No	Yes	No	Yes	No	Yes	Yes	Yes
Oral Rat Acute Toxicity (LD50) mol/kg	2.42	1.78	2.65	2.39	2.02	2.36	2.01	2.56	2.48	2.66	2.37	2.35	2.43	2.22	2.59

can bind to Gly38. Compared to CY13, the methoxy substitution at C6 slightly lowers the potency. This replacement of the methoxy group results in the loss of conventional hydrogen bonds with Gly37 and changes to carbon-hydrogen bonds. Compared with CY5, it was seen that the loss of hydroxy substituents resulted in the absence of conventional hydrogen bonds with Gly37.

The following comparison can be seen between groups A and B. Interestingly, the difference in the position of the dimethyl chromene group affects the potency of inhibitory activity. When CY6 was compared with CY12 (IC_{50} 180.2 μM), it was seen that a shift in the position of the dimethyl chromene ring resulted in a decrease in potency. On confirmation of the docking simulation, although CY12 can form hydrogen bonds from hydroxy 5 with Gly37, CY12 loses its bond with Gly38. Furthermore, in comparing CY12 and CY1, replacing the hydroxy substituent in group B with methoxy shows a lowers potency. The docking result confirms that CY1 lost the H-bond with the Gly37 due to the change of the hydroxyl group with the methoxy group. In general, it can be concluded that group B flavonoid has a lower potential than group A.

The compound with the highest activity in group C is CY14 (IC_{50} 105.5 μM). Compared with CY2 (IC_{50} 195.3 μM), the result indicates that the different position of the furan ring between the two compounds affects the compound's activity. Confirmation using molecular docking showed that both CY2 and CY14 could bind to the hydrophobic central and C terminal hydrophobic. However, CY14 has an additional carbon-hydrogen bond on Leu17, which might lead to increased activity of CY14 over CY2. In addition, CY10 has a lower activity than CY14. Furthermore, if a comparison is made between CY 1 from group B and CY 2 from group C, replacing the dimethyl chromene ring with furan can increase the activity. Group C compounds generally have better activity than group B but are lower than group A. In group D, all compounds show $IC_{50} > 200$ μM. This result indicates that group D (furanochalcone) generally has a lower activity than groups A, B, or C.

In the in vitro cell culture model, we use the H_2O_2 induce model to study AD-related activity. The prooxidant H_2O_2 promotes Aβ production through JNK-dependent activation of γ-secretase [31]. The APP processing is sequential proteolysis carried out by β- and γ-secretase, leading to the generation of Aβ and neurotoxicity [32]. H_2O_2 induced Aβ production through enhancement of γ-secretase activation, resulting in the promotion of APP cleavage. H_2O_2 caused a significant increase in AICD without inhibiting AICD degradation [5]. Another source of H_2O_2 might be the progression of Aβ aggregation [33]. Escalated Aβ accumulation and microglial activation induce a high level of ROS, including endogenous H_2O_2 [34]. Excessive ROS stimulates JNK activity in susceptible neurons that surround the amyloid plaques. Such exacerbation of a vicious cycle may explain how the process of AD pathology becomes accelerated and irreversible at the modest and late AD stage [35]. From the in vitro cell culture model, the result shows that all flavonoid is not toxic in the dose of 10 μM. All the flavonoids also show neuroprotective effects against H_2O_2 toxicity. The compound with the highest neuroprotective effect is CY9. However, this compound does not show the multifunction product in BuChE and anti-aggregation AB. Interestingly, CY6 shows a multifunctional effect, is predicted to have ideal physic chemistry, and does not have toxicity. Thus, CY9 and CY6 tested the neuroprotective effect with various doses. The findings suggested that CY9 and CY6 significantly protect differentiated SH-SY5Y cells from H_2O_2 damage in a dose-dependent manner.

In ADMET screening, 15 compounds were analyzed using the pKCSM tool. The predicted parameters are absorption, distribution, metabolism, excretion, and toxicity. The table shows that all compounds have intestinal absorption percentage values of more than 30 %, indicating that all are easily absorbed [36]. The highest absorption value was CY10 (98.547 %), and the lowest was CY9 (87.022 %). Thus, all flavonoids have good intestinal absorption.

Regarding distribution indicators, the parameters used are BBB permeability and CNS permeation. The standard value of a compound having a good BBB is more than 0.3 and is considered to have a low BBB if it is less than −1. CNS permeation is said to be good if the log PS value is > -2, and if the log PS value is < -3, it is considered unable to penetrate the CNS [37]. From the results of BBB permeability prediction, it is known that all compounds have a value > −1, indicating that all compounds can pass BBB, even some compounds such as CY1, CY2, CY4, CY5, CY9, CY12, and CY13 have values > 0.3 which means they have BBB permeability the good one. Furthermore, in the CNS penetration parameter, it is known that all compounds have a value of < -3, so it is known that all compounds can penetrate the CNS.

Furthermore, on the metabolic parameters, the cytochrome P450 model was used. This enzyme is important for the body in the phase 1 metabolic process of xenobiotics and makes it easier for them to be excreted out of the body. Of the approximately 17 types of CYPs identified, only about 4 CYPs (1A2, 2C9, 2C19, 2D6, and 3A4) [38] are involved in 90 % of first-pass drug metabolism. Of the four, 2D6 and 3A4 are the most dominant. Based on the prediction results, it is known that all compounds are CYP3A4 substrates and not 2D6 substrates. This indicates that the increase in CYP3A4 activity and levels will affect the metabolism of these flavonoids. Furthermore, the analysis of CYP inhibitors showed that CY1, CY2, CY5, CY6, CY8, CY11, CY12, and CY14 were CYP3A4 inhibitors, while CY2 were CYP2D6 inhibitors. The excretory parameters predicted the clearance value and renal OCT2 substrate (organic cation transporter 2). If a compound is an OCT2 substrate, it has the potential for adverse interaction with an OCT2 inhibitor. From the prediction results, it is known that the flavonoid clearance value ranges from 0.182 to 0.804. Some compounds have OCT2 substrate properties including CY1, CY4, CY10, CY12 and CY13. The next parameter is the potential for toxicity based on the prediction of hepatotoxicity, AMES test, and LD50 [39]. From the prediction results, several compounds appear to have hepatotoxic potential, namely CY5, CY11, CY13, and CY15. AMES test parameters were used to predict the potential mutagenicity of compounds. Some compounds with mutagenic potential are CY2, CY5, CY9, CY11, CY13, CY14, and CY15. The LD50 value of flavonoids ranges from 1.78 mol/kg to 2.66 mol/kg.

4. Materials and methods

4.1. Flavonoid derivatives

The isolation and elucidation of flavonoid derivatives from *M. brandisiana* root were reported elsewhere [40]. The fifteen flavonoids include 5-methoxy-6″,6″-dimethylchromeno-[2″,3″:7,6]-flavone (CY1), pinnatin (CY2), pongamol (CY3), isopongaflavone (CY4), 6″,6″-dimethylchromeno-[2″,3″:7,8]-flavone (CY5), candidine (CY6), ovalitenin A (CY7), 2′-methoxy-6″,6″-dimethylchromeno-[2″,3″:4′, 3′]-*β*-hydroxychalcone (CY8), O-methylpongamol (CY9), 3,3′,4′,7-tetra-O-methyl fisetin (CY10), brandisianone B (CY11), 5-hydroxy-6″,6″-dimethylchromeno-[2″,3″:7,6]-flavone(CY12), 6-methoxy-6″,6″-dimethylchromeno-[2″,3″:7,8]flavone (CY13), lanceolatin B (CY14), brandisianone F (CY15).

4.2. In silico prediction of the drug-likeness properties

The Swiss ADME software was used to evaluate physicochemical parameters to identify good drug candidates [41]. All test compounds were characterized for their physicochemical properties, including molecular weight, topological polar surface area (TPSA), number of rotatable bonds, number of H-bond acceptors, number of H-bond donors, and lipophilicity. Lipinski and Veber's rules were applied to verify the drug-likeness profile.

4.3. Amyloid aggregation inhibitory activity

Aβ $_{1\text{-}42}$ aggregation inhibition was tested, as previously described [42]. Briefly, the test compound at various concentrations (0–200 μM) was mixed with 9 μL of 25 μM $A\beta_{1-42}$ in 50 mM phosphate buffer, pH 7.4. Next, following with incubation at 37 °C for 48 h in the dark, the sample was combined with 50 μM glycine/NaOH buffer (pH 8.5) which containing 5 μM ThT. Fluorescence intensities were measured at 446 nm for excitation and 490 nm for emission. Following the measurement of the fluorescence intensity, the percentage of inhibition on aggregation was determined using the equation:

$$\text{Percentage of inhibition} = (1 - \text{IFi/IFc}) * 100\%$$

The concentration that inhibits Aβ $_{1\text{-}42}$ aggregation by 50 % (IC_{50}) was determined using a concentration-inhibition linear regression analysis for each chemical. Independent triplicates of the experiment were performed.

4.4. In vitro BuChE inhibitory activity

Ellman's method [43] was slightly modified to evaluate the enzyme activity inhibition of BuChE. The assay mixture contains 25 μl of 0.1 M phosphate buffer (pH 7.4), 25 μl of 1 mM substrate (butyryl thiocholine iodide solution), 125 μl of 1 mM 5, 5′-dithiobis-(2 nitrobenzoic acid (DTNB), 50 μl of 0.2 Units/mL BuChE, and 25 μl of the test inhibitor stock solutions. The enzyme activity was assessed using a METERTECH Accureader M965 microplate reader by recording the increase in absorbance at 405 nm over the duration of 5 min. All experiments were done in triplicate.

4.5. Neuroprotective effect against H_2O_2-induced cell death

SH-SY5Y neuroblastoma cells were cultured in DMEM/F12 with 10 % FBS at 37 °C in a humidified 5 % CO_2 incubator. The cells were seeded in a 96-well plate for the tests at a 5×10^5 cells/mL density in 100 μL DMEM with FBS 10 % and allowed to attach for 48 h. Two days after seeding, cells were differentiated with 10 μM retinoic acid, FBS 1 % for six days before treatment. For toxicity screening, the cells were exposed to curcumin or fifteen flavonoid derivatives at concentrations of 0.1 μM, 1 μM, 10 μM, and 100 μM for 24 h to determine their cytotoxicity. The cells were stained for 2 h with MTT (5 mg/mL in PBS) and 3-(4, 5-dimethyl-2-thiazolyl)-2, 5-diphenyl-2H-tetrazolium bromide to measure cell viability. A METERTECH Accureader M965 microplate reader was utilized to measure the optical density of each well at 550 nm. To investigate neuroprotective activity against H_2O_2, the differentiated neuroblastoma cells were pretreated with flavonoid derivatives or curcumin as a standard at varied doses for 2 h. Following the removal of unabsorbed test chemicals by phosphate buffer saline washing. Next, oxidative stress was generated in the cells for 3 h using 250 μM H_2O_2. To assess cell viability, MTT was utilized. In a microplate reader, the optical density of each well was determined at 550 nm. The outcome shows a comparison of the samples group and the negative group's cell viability in percentage. The following equation was used to determine the percentage of viable cells:

$$\%\text{Cell viability} = (100 \times \text{A1})/\text{A0} \qquad \text{A0}$$

4.6. Molecular docking

To create the target templates Aβ1-42 and BuChE, water and other solvent molecules were removed, all hydrogens were added, Gasteiger charges were given, and non-polar hydrogen atoms were combined. The X-ray crystal PDB codes 2BEG and 1P0I were used to

construct the Aβ fibril and BuChE, respectively [44,45]. Grid maps were generated using AutoGrid 4. The grids were designed to contain the active site of BuChE and the whole structure of fibril A. For BuChE and Aβ fibrils, the grid box dimensions were established with sizes of 80 × 70 × 70 Å and 120 × 60 × 40 Å, respectively, and 0.375-unit grid spacing was used. The AutoDock 4.2.6 software was used to dock all ligands using the Lamarckian genetic method [46,47]. For the Lamarckian genetic algorithm technique, it was set to use a population size of 100 individuals and 100 ligand orientation runs. The maximum number of evaluations was 27,000, and the energy evaluation was 1,000,000. The conformation with the lowest docked energy was chosen as best. Using BIOVIA Discovery Studio 2017, the docking complex postures were examined for interactions after the docking procedure [48,49].

4.7. Molecular dynamic simulation

The molecular dynamic simulation was performed using Google Compute Engine backend (GPU)Python 3; the allotted GPU nodes are NVIDIA-SMI 525.85.12, Driver Version: 525.85.12, and CUDA Version: 12.0. The top four high scores IC50 of CY in BuChE inhibition were submitted to MD simulation tests using Open MM to evaluate their binding stability [50]. AMBER Tools neutralize the system and create protein and ligand structure ff19SB and GAFF2 force fields [51]. In the TIP3P water model, apo BuChE (unbound) and the BuChE-compound complex were produced and solvated, then neutralized by adding NaCl ions. Before conducting MDS, its concentration was fixed at 0.15 M. Following equilibration, the production MD simulation was run for 50 ns at 310 K and 1 bar. The frequency at which the trajectory and log file was written was set to 10 ps, and MDs production was aligned and concatenated in the. dcd file with eliminated water. To determine the stability of protein-ligand complexes, measures such as root mean square deviation (RMSD), root mean square fluctuation (RMSF), the radius of gyration (Rg), MM/GBSA (Molecular mechanics generalized born and surface area), and Principal component analysis (PCA) were examined.

4.8. In silico drug ADMET evaluation

To predict the pharmacokinetic parameters of flavonoid derivatives, pKCSM software was used [52]. This software can predict ADMET parameters. The absorption parameters that can be predicted are human intestinal absorption and Caco2 permeability. Blood-brain barrier (BBB) and central nervous system (CNS) permeability parameters can be predicted for distribution parameters. The brain distribution is assessed by the blood-brain barrier (log BB) permeability. Metabolism is predicted based on the CYP inhibition model, including CYP2C9 and CYP3A4. Excretion is predicted based on the total clearance and renal OCT2 substrate. The toxicity of drugs is predicted based on the hepatotoxicity and maximum tolerated dose (human) [53].

4.9. Statistical analysis

The results were expressed as mean ± SD (n = 4–6). Statistical significance was performed by one-way analysis of variance (ANOVA) followed by the Tukey post hoc test. For all statistical analyses, $p < 0.05$ was accepted as statistically significant.

5. Conclusions

To summarize, 15 flavonoids from *Millettia brandisiana,* namely 5-methoxy-6″,6″-dimethylchromeno-[2″,3″:7,6]-flavone (CY1), pinnatin (CY2), pongamol (CY3), isopongaflavone (CY4), 6″,6″-dimethylchromeno-[2″,3″:7,8]-flavone (CY5), candidine (CY6), ovalitenin A (CY7), 2′-methoxy-6″,6″-dimethylchromeno-[2″,3″:4′,3′]-*β*-hydroxychalcone (CY8), O-methylpongamol (CY9), 3,3′,4′,7-tetra-O-methyl fisetin (CY10), brandisianone B (CY11), 5-hydroxy-6″,6″-dimethylchromeno-[2″,3″:7,6]-flavone (CY12), 6-methoxy-6″,6″-dimethylchromeno-[2″,3″:7,8]flavone (CY13), lanceolatin B (CY14), brandisianone F (CY15) were evaluated for the multifunctional effect against AD pathogenesis including BuChE inhibition, anti-Aβ aggregation, and neuroprotection. The results show that six flavonoids have potency in BuChE inhibition, and four flavonoids show potency in the anti-Aβ collection. The structure-activity relationship also was discussed in this study. Flavonoids with the 6″,6″-dimethylchromeno-[2″,3″:7,8]-flavone skeleton show the best multifunctional effect. Prediction of drug-likeness properties shows that all flavonoids fit the requirement. pKCSM programs were used to predict ADMET parameters for all the flavonoids. Taken together, candidine shows the best multifunctional effect, proper drug-likeness properties, and ADMET parameters. In addition, candidine also can prevent neuronal damage induced by H_2O_2. Thus, candidine can be considered as a candidate for AD treatment. However, the mechanism of action at the cellular level is the next important step that should be studied in the future.

Author contributions

Conceived and designed the experiments, P·W., C·Y., O.M., N·N., and C·B.; analyzed and interpreted the data, P.A., P.W. and C·B.; performed the experiments, P.A., S.A., P.T., P·W., and C·B.; contributed reagents, materials, analysis tools or data, C·B., P·W., and C·Y.; wrote the paper, P.A., P.W. and C·B.; project administration, C·B.; All authors have read and agreed to the published version of the manuscript.

Funding

This research was funded by the Fundamental Fund of Khon Kaen University under the National Science, Research and Innovation

Fund; Faculty of Pharmaceutical Sciences, Khon Kaen University; Research and Graduate Studies, Khon Kaen University; Research Program, Khon Kaen University; and Ubon Ratchathani University, Thailand.

Institutional review board statement

Not applicable.

Informed consent statement

Not applicable.

Data availability statement

Data is contained within the article.

Declaration of competing interest

The authors declare that they have no known competing financial interests or personal relationships that could have appeared to influence the work reported in this paper.

Appendix A. Supplementary data

Supplementary data to this article can be found online at https://doi.org/10.1016/j.heliyon.2023.e21894.

References

[1] S. Tiwari, V. Atluri, A. Kaushik, A. Yndart, M. Nair, Alzheimer's disease: pathogenesis, diagnostics, and therapeutics, IJN 14 (2019) 5541–5554, https://doi.org/10.2147/IJN.S200490.
[2] X. Du, X. Wang, M. Geng, Alzheimer's disease hypothesis and related therapies, Transl. Neurodegener. 7 (2018) 2, https://doi.org/10.1186/s40035-018-0107-y.
[3] P.H. Reddy, M.F. Beal, Amyloid beta, mitochondrial dysfunction and synaptic damage: implications for cognitive decline in aging and alzheimer's disease, Trends Mol. Med. 14 (2008) 45–53, https://doi.org/10.1016/j.molmed.2007.12.002.
[4] S. Kumar, J. Walter, Phosphorylation of amyloid beta (Aβ) peptides – a trigger for formation of toxic aggregates in alzheimer's disease, Aging 3 (2011) 803–812, https://doi.org/10.18632/aging.100362.
[5] C. Cheignon, M. Tomas, D. Bonnefont-Rousselot, P. Faller, C. Hureau, F. Collin, Oxidative stress and the amyloid beta peptide in alzheimer's disease, Redox Biol. 14 (2018) 450–464, https://doi.org/10.1016/j.redox.2017.10.014.
[6] Q. Li, H. Yang, Y. Chen, H. Sun, Recent progress in the identification of selective butyrylcholinesterase inhibitors for alzheimer's disease, Eur. J. Med. Chem. 132 (2017) 294–309, https://doi.org/10.1016/j.ejmech.2017.03.062.
[7] M.-M. Mesulam, A. Guillozet, P. Shaw, A. Levey, E.G. Duysen, O. Lockridge, Acetylcholinesterase knockouts establish central cholinergic pathways and can use butyrylcholinesterase to hydrolyze acetylcholine, Neuroscience 110 (2002) 627–639, https://doi.org/10.1016/S0306-4522(01)00613-3.
[8] G. Mushtaq, N. Greig, J. Khan, M. Kamal, Status of acetylcholinesterase and butyrylcholinesterase in Alzheimer's disease and type 2 diabetes mellitus, CNSNDDT 13 (2014) 1432–1439, https://doi.org/10.2174/1871527313666141023141545.
[9] N.H. Greig, T. Utsuki, Q.-S. Yu, X. Zhu, H.W. Holloway, T. Perry, B. Lee, D.K. Ingram, D.K. Lahiri, A new therapeutic target in alzheimer's disease treatment: attention to butyrylcholinesterase, Curr. Med. Res. Opin. 17 (2001) 159–165, https://doi.org/10.1185/03007990152673800.
[10] A. Shafferman, C. Kronman, Y. Flashner, M. Leitner, H. Grosfeld, A. Ordentlich, Y. Gozes, S. Cohen, N. Ariel, D. Barak, Mutagenesis of human acetylcholinesterase. Identification of residues involved in catalytic activity and in polypeptide folding, J. Biol. Chem. 267 (1992) 17640–17648, https://doi.org/10.1016/S0021-9258(19)37091-7.
[11] M. Bajda, A. Więckowska, M. Hebda, N. Guzior, C. Sotriffer, B. Malawska, Structure-based search for new inhibitors of cholinesterases, Indian J. Manag. Sci. 14 (2013) 5608–5632, https://doi.org/10.3390/ijms14035608.
[12] Y. Nicolet, O. Lockridge, P. Masson, J.C. Fontecilla-Camps, F. Nachon, Crystal structure of human butyrylcholinesterase and of its complexes with substrate and products, J. Biol. Chem. 278 (2003) 41141–41147, https://doi.org/10.1074/jbc.M210241200.
[13] Y. Dong, X. Li, J. Cheng, L. Hou, Drug development for alzheimer's disease: microglia induced neuroinflammation as a target? Indian J. Manag. Sci. 20 (2019) 558, https://doi.org/10.3390/ijms20030558.
[14] C.-X. Gong, C.-L. Dai, F. Liu, K. Iqbal, Multi-targets: an unconventional drug development strategy for alzheimer's disease, Front. Aging Neurosci. 14 (2022), 837649, https://doi.org/10.3389/fnagi.2022.837649.
[15] L. Jalili-Baleh, E. Babaei, S. Abdpour, S. Nasir Abbas Bukhari, A. Foroumadi, A. Ramazani, M. Sharifzadeh, M. Abdollahi, M. Khoobi, A review on flavonoid-based scaffolds as multi-target-directed ligands (MTDLs) for alzheimer's disease, Eur. J. Med. Chem. 152 (2018) 570–589, https://doi.org/10.1016/j.ejmech.2018.05.004.
[16] M. Sato, K. Murakami, M. Uno, Y. Nakagawa, S. Katayama, K. Akagi, Y. Masuda, K. Takegoshi, K. Irie, Site-specific inhibitory mechanism for amyloid B42 aggregation by catechol-type flavonoids targeting the Lys residues, J. Biol. Chem. 288 (2013) 23212–23224, https://doi.org/10.1074/jbc.M113.464222.
[17] E.Y. Choi, S.S. Kang, S.K. Lee, B.H. Han, Polyphenolic biflavonoids inhibit amyloid-beta fibrillation and disaggregate preformed amyloid-beta fibrils, Biomolecules & Therapeutics 28 (2020) 145–151, https://doi.org/10.4062/biomolther.2019.113.
[18] K. Andrich, J. Bieschke, The effect of (−)-Epigallo-Catechin-(3)-Gallate on amyloidogenic proteins suggests a common mechanism, in: N. Vassallo (Ed.), Natural Compounds as Therapeutic Agents for Amyloidogenic Diseases vol. 863, Advances in Experimental Medicine and Biology; Springer International Publishing, Cham, 2015, pp. 139–161. ISBN 978-3-319-18364-0.
[19] R. Jena, D. Rath, S.S. Rout, D.M. Kar, A review on genus Millettia: traditional uses, phytochemicals and pharmacological activities, Saudi Pharmaceut. J. 28 (2020) 1686–1703, https://doi.org/10.1016/j.jsps.2020.10.015.
[20] O. Pancharoen, A. Athipornchai, A. Panthong, W.C. Taylor, Isoflavones and rotenoids from the leaves of Millettia brandisiana, Chem. Pharm. Bull. 56 (2008) 835–838, https://doi.org/10.1248/cpb.56.835.

[21] P. Pailee, C. Mahidol, S. Ruchirawat, V. Prachyawarakorn, Diverse flavonoids from the roots of Millettia brandisiana, Phytochemistry 162 (2019) 157–164, https://doi.org/10.1016/j.phytochem.2019.03.013.

[22] C.A. Lipinski, F. Lombardo, B.W. Dominy, P.J. Feeney, Experimental and computational approaches to estimate solubility and permeability in drug discovery and development settings 1PII of original article: S0169-409x(96)00423-1. The article was originally published in advanced drug delivery reviews 23 (1997) 3–25. 1, Adv. Drug Deliv. Rev. 46 (2001) 3–26, https://doi.org/10.1016/S0169-409X(00)00129-0.

[23] D.F. Veber, S.R. Johnson, H.-Y. Cheng, B.R. Smith, K.W. Ward, K.D. Kopple, Molecular properties that influence the oral bioavailability of drug candidates, J. Med. Chem. 45 (2002) 2615–2623, https://doi.org/10.1021/jm020017n.

[24] R. Hussain, F. Rahim, W. Rehman, M. Taha, S. Khan, K. Zaman, S.A. Ali Shah, A. Wadood, S. Imran, M. Abdellatif, New bis-thiazolidinone based chalcone analogues as effective inhibitors of alzheimer's disease: synthesis, molecular docking, acetylcholinesterase and butyrylcholinesterase study, Chem. Biodivers. (2022), 202200323, https://doi.org/10.1002/cbdv.202200323 cbdv.

[25] M. Katalinić, G. Rusak, J. Domaćinović Barović, G. Šinko, D. Jelić, R. Antolović, Z. Kovarik, Structural aspects of flavonoids as inhibitors of human butyrylcholinesterase, Eur. J. Med. Chem. 45 (2010) 186–192, https://doi.org/10.1016/j.ejmech.2009.09.041.

[26] J.-P. Guo, T. Arai, J. Miklossy, P.L. McGeer, Abeta and tau form soluble complexes that may promote self aggregation of both into the insoluble forms observed in alzheimer's disease, a 103 (2006) 1953–1958, https://doi.org/10.1073/pnas.0509386103.

[27] G. Chen, T. Xu, Y. Yan, Y. Zhou, Y. Jiang, K. Melcher, H.E. Xu, Amyloid beta: structure, biology and structure-based therapeutic development, Acta Pharmacol. Sin. 38 (2017) 1205–1235, https://doi.org/10.1038/aps.2017.28.

[28] M.P. Murphy, H. LeVine, Alzheimer's disease and the amyloid-β peptide, JAD 19 (2010) 311–323, https://doi.org/10.3233/JAD-2010-1221.

[29] T. Lührs, C. Ritter, M. Adrian, D. Riek-Loher, B. Bohrmann, H. Döbeli, D. Schubert, R. Riek, 3D structure of alzheimer's amyloid-beta(1-42) fibrils, Proc. Natl. Acad. Sci. U.S.A. 102 (2005) 17342–17347, https://doi.org/10.1073/pnas.0506723102.

[30] B. Urbanc, L. Cruz, S. Yun, S.V. Buldyrev, G. Bitan, D.B. Teplow, H.E. Stanley, *In silico* study of amyloid β-protein folding and oligomerization, Proc. Natl. Acad. Sci. U.S.A. 101 (2004) 17345–17350, https://doi.org/10.1073/pnas.0408153101.

[31] E. Tamagno, M. Guglielmotto, M. Aragno, R. Borghi, R. Autelli, L. Giliberto, G. Muraca, O. Danni, X. Zhu, M.A. Smith, et al., Oxidative stress activates a positive feedback between the γ- and β-secretase cleavages of the β-amyloid precursor protein, J. Neurochem. (2007), https://doi.org/10.1111/j.1471-4159.2007.05072.x, 0, 071115163316002-???

[32] C. Haass, C. Kaether, G. Thinakaran, S. Sisodia, Trafficking and proteolytic processing of APP, Cold Spring Harbor Perspectives in Medicine 2 (2012), https://doi.org/10.1101/cshperspect.a006270 a006270–a006270.

[33] B.J. Tabner, O.M.A. El-Agnaf, S. Turnbull, M.J. German, K.E. Paleologou, Y. Hayashi, L.J. Cooper, N.J. Fullwood, D. Allsop, Hydrogen peroxide is generated during the very early stages of aggregation of the amyloid peptides implicated in alzheimer disease and familial British dementia, J. Biol. Chem. 280 (2005) 35789–35792, https://doi.org/10.1074/jbc.C500238200.

[34] F.L. Andronie-Cioara, A.I. Ardelean, C.D. Nistor-Cseppento, A. Jurcau, M.C. Jurcau, N. Pascalau, F. Marcu, Molecular mechanisms of neuroinflammation in aging and alzheimer's disease progression, Indian J. Manag. Sci. 24 (2023) 1869, https://doi.org/10.3390/ijms24031869.

[35] C. Shen, Y. Chen, H. Liu, K. Zhang, T. Zhang, A. Lin, N. Jing, Hydrogen peroxide promotes Aβ production through JNK-dependent activation of γ-secretase, J. Biol. Chem. 283 (2008) 17721–17730, https://doi.org/10.1074/jbc.M800013200.

[36] T. Hou, J. Wang, W. Zhang, X. Xu, ADME evaluation in drug discovery. 7. Prediction of oral absorption by correlation and classification, J. Chem. Inf. Model. 47 (2007) 208–218, https://doi.org/10.1021/ci600343x.

[37] C. Suenderhauf, F. Hammann, J. Huwyler, Computational prediction of blood-brain barrier permeability using decision tree induction, Molecules 17 (2012) 10429–10445, https://doi.org/10.3390/molecules170910429.

[38] F. Cheng, W. Li, Y. Zhou, J. Shen, Z. Wu, G. Liu, P.W. Lee, Y. Tang, AdmetSAR: a comprehensive source and free tool for assessment of chemical ADMET properties, J. Chem. Inf. Model. 52 (2012) 3099–3105, https://doi.org/10.1021/ci300367a.

[39] D. Fourches, J.C. Barnes, N.C. Day, P. Bradley, J.Z. Reed, A. Tropsha, Cheminformatics analysis of assertions mined from literature that describe drug-induced liver injury in different species, Chem. Res. Toxicol. 23 (2010) 171–183, https://doi.org/10.1021/tx900326k.

[40] S. Arthan, C. Pornchoo, A. Prawan, S. Tontapha, V. Amornkitbamrung, C. Yenjai, Brandisianones F and G from *Millettia brandisiana* kurz and their cytotoxicity, Nat. Prod. Res. (2021) 1–9, https://doi.org/10.1080/14786419.2020.1869971.

[41] A. Daina, O. Michielin, V. Zoete, SwissADME: a free web tool to evaluate pharmacokinetics, drug-likeness and medicinal chemistry friendliness of small molecules, Sci. Rep. 7 (2017), 42717, https://doi.org/10.1038/srep42717.

[42] H. LeVine, [18] quantification of β-sheet amyloid fibril structures with thioflavin T, in: Methods in Enzymology, vol. 309, Elsevier, 1999, pp. 274–284. ISBN 978-0-12-182210-1.

[43] G.L. Ellman, K.D. Courtney, V. Andres, R.M. Featherstone, A new and rapid colorimetric determination of acetylcholinesterase activity, Biochem. Pharmacol. 7 (1961) 88–95, https://doi.org/10.1016/0006-2952(61)90145-9.

[44] T. Lührs, C. Ritter, M. Adrian, D. Riek-Loher, B. Bohrmann, H. Döbeli, D. Schubert, R. Riek, 3D structure of alzheimer's amyloid-β(1–42) fibrils, Proc. Natl. Acad. Sci. U.S.A. 102 (2005) 17342–17347, https://doi.org/10.1073/pnas.0506723102.

[45] Y. Nicolet, O. Lockridge, P. Masson, J.C. Fontecilla-Camps, F. Nachon, Crystal structure of human butyrylcholinesterase and of its complexes with substrate and products, J. Biol. Chem. 278 (2003) 41141–41147, https://doi.org/10.1074/jbc.M210241200.

[46] G.M. Morris, D.S. Goodsell, R.S. Halliday, R. Huey, W.E. Hart, R.K. Belew, A.J. Olson, Automated docking using a lamarckian genetic algorithm and an empirical binding free energy function, J. Comput. Chem. 19 (1998) 1639–1662, https://doi.org/10.1002/(SICI)1096-987X(19981115)19:14<1639::AID-JCC10>3.0.CO;2-B.

[47] A. Meden, D. Knez, N. Malikowska-Racia, X. Brazzolotto, F. Nachon, J. Svete, K. Sałat, U. Grošelj, S. Gobec, Structure-activity relationship study of tryptophan-based butyrylcholinesterase inhibitors, Eur. J. Med. Chem. 208 (2020), 112766, https://doi.org/10.1016/j.ejmech.2020.112766.

[48] D.V. Pedersen, T.A.F. Gadeberg, C. Thomas, Y. Wang, N. Joram, R.K. Jensen, S.M.M. Mazarakis, M. Revel, C. El Sissy, S.V. Petersen, et al., Structural basis for properdin oligomerization and convertase stimulation in the human complement system, Front. Immunol. 10 (2019) 2007, https://doi.org/10.3389/fimmu.2019.02007.

[49] P. Takomthong, P. Waiwut, C. Yenjai, B. Sripanidkulchai, P. Reubroycharoen, R. Lai, P. Kamau, C. Boonyarat, Structure–activity analysis and molecular docking studies of coumarins from toddalia asiatica as multifunctional agents for alzheimer's disease, Biomedicines 8 (2020) 107, https://doi.org/10.3390/biomedicines8050107.

[50] P. Eastman, J. Swails, J.D. Chodera, R.T. McGibbon, Y. Zhao, K.A. Beauchamp, L.-P. Wang, A.C. Simmonett, M.P. Harrigan, C.D. Stern, et al., OpenMM 7: rapid development of high performance algorithms for molecular dynamics, PLoS Comput. Biol. 13 (2017), e1005659, https://doi.org/10.1371/journal.pcbi.1005659.

[51] C. Tian, K. Kasavajhala, K.A.A. Belfon, L. Raguette, H. Huang, A.N. Migues, J. Bickel, Y. Wang, J. Pincay, Q. Wu, et al., Ff19SB: amino-acid-specific protein backbone parameters trained against quantum mechanics energy surfaces in solution, J. Chem. Theor. Comput. 16 (2020) 528–552, https://doi.org/10.1021/acs.jctc.9b00591.

[52] P. Takomthong, P. Waiwut, C. Yenjai, A. Sombatsri, P. Reubroycharoen, L. Lei, R. Lai, S. Chaiwiwatrakul, C. Boonyarat, Multi-target actions of acridones from atalantia monophylla towards alzheimer's pathogenesis and their pharmacokinetic properties, Pharmaceuticals 14 (2021) 888, https://doi.org/10.3390/ph14090888.

[53] D.E.V. Pires, T.L. Blundell, D.B. Ascher, PkCSM: predicting small-molecule pharmacokinetic and toxicity properties using graph-based signatures, J. Med. Chem. 58 (2015) 4066–4072, https://doi.org/10.1021/acs.jmedchem.5b00104.